

Suitability of ground-based SfM-MVS for monitoring glacial and periglacial processes

L. Piermattei¹, L. Carturan¹, F. de Blasi¹, P. Tarolli¹, G. Dalla Fontana¹, A. Vettore² and N. Pfeifer³.

¹Department of Land, Environment, Agriculture and Forestry, University of Padova, Italy

²Interdepartment Research Center of Geomatics, University of Padova, Italy

³Department of Geodesy and Geoinformation, TU Wien, Austria

Correspondence to: L. Piermattei (livia.piermattei@studenti.unipd.it)

Abstract

Photo-based surface reconstruction is rapidly emerging as an alternative survey technique to LiDAR (light detection and ranging) in many fields of geoscience fostered by the recent development of computer vision algorithms such as Structure from Motion (SfM) and dense image matching such as Multi-View Stereo (MVS). The objective of this work was to test the suitability of the ground-based SfM-MVS approach in calculating the geodetic mass balance of a 2.1 km² glacier and for the detection of the surface displacement rate of a neighbouring active rock glacier located in the Eastern Italian Alps. The photos were acquired in 2013 and 2014 using a digital consumer-grade camera, organizing single-day field surveys. Airborne laser scanning (ALS) data were used as benchmarks to estimate the accuracy of the photogrammetric digital elevation models (DEMs) and the reliability of the method. The SfM-MVS approach enabled the reconstruction of high-quality DEMs, which provided estimates of glacial and periglacial processes similar to those achievable by ALS. In stable bedrock areas outside the glacier, the mean and the standard deviation of the elevation difference between the SfM-MVS DEM and the ALS DEM was $-0.42 \text{ m} \pm 1.72 \text{ m}$ and $0.03 \text{ m} \pm 0.74 \text{ m}$ in 2013 and 2014, respectively. In the rock glacier area, the elevation difference was $0.02 \text{ m} \pm 0.17 \text{ m}$. The use of natural targets as ground control points, the occurrence of shadowed and low-contrast areas, and in particular the sub-optimal camera network geometry imposed by the morphology of the study area were the main factors affecting the accuracy of photogrammetric DEMs.

34 **1. Introduction**

35 Knowledge of changes in the extent, mass and surface velocity of glaciers and rock
36 glaciers contributes to better understanding the dynamic processes occurring in cold
37 high-mountain environments and serves as an important contribution to climate
38 monitoring (Kääb et al., 2003).

39 Numerous techniques exist for monitoring and quantifying these changes and include
40 both field and remote sensing methods (Immerzeel et al., 2014). Fieldwork generally
41 yields high-quality data but with a small spatial extent, given the remoteness and low
42 accessibility of mountain areas at high elevations (Roer et al., 2007). Therefore,
43 using remotely sensed datasets for at least two different points in time has become
44 an important tool for monitoring high-mountain terrain dynamics (Kääb, 2002).
45 Multitemporal Digital Elevation Models (DEMs) based on remote sensing data are the
46 most commonly used products for such investigations (Kääb, 2005; Tseng et al.,
47 2015).

48 Among the available remote sensing techniques, the close-range photogrammetry
49 saw a rapid development thanks to the recent evolution of digital photogrammetry,
50 based on computer vision algorithms. This technique is becoming the major
51 alternative to traditional surveying techniques and LiDAR (light detection and
52 ranging) technologies, due to its lower cost, high portability, and easy and rapid
53 surveying in the field.

54 The photogrammetric approach known as Structure from Motion (SfM) allows
55 obtaining 3D information of the photographed object from a sequence of overlapping
56 images taken with a digital camera.

57 A limited number of applications of SfM photogrammetry in glacial and periglacial
58 environments exists, and they principally involve the use of Unmanned Aerial
59 Vehicles (UAVs) for image acquisition (Solbø S. and Storvold R. 2013; Whitehead et
60 al., 2013; Immerzeel et al., 2014, Tonkin et al., 2014; Gauthier et al., 2014; Bühler et
61 al., 2014; Dall'Asta et al., 2015; Ryan et al., 2015) rather than ground-based surveys
62 (Gómez-Gutiérrez et al., 2014; 2015; Kääb et al., 2014; Piermattei et al., 2015).

63 The objective of our work was to assess the suitability of the ground-based SfM
64 approach for monitoring glacial and periglacial processes in a high-altitude area of
65 the Ortles-Cevedale Group (Eastern Italian Alps). In particular, this approach was
66 used to calculate the geodetic annual mass balance of a 2.1 km² glacier and to
67 detect the surface displacement of a neighbouring 0.06 km² rock glacier. The

68 photogrammetric surveys were intentionally planned to be as quick and cost-effective
69 as possible, and easily replicable in the future. Therefore, a consumer-grade camera
70 was adopted to find an appropriate balance between the affordability and
71 accessibility of the system (i.e. cost and ease of use) and the quality of the resulting
72 topographic data (accuracy and density). The accuracy of the photogrammetric
73 DEMs was estimated using ALS-based DEMs acquired during the same periods. The
74 main factors affecting the accuracy of the photogrammetric DEMs were investigated,
75 and the significance of the biases in the quantification of glacial and periglacial
76 processes was discussed.

77

78 **2. Geographical setting and case studies**

79 The La Mare Glacier and the neighbouring AVDM3 Rock Glacier are located in the
80 south-eastern part of the Ortles-Cevedale massif (Eastern Italian Alps), the largest
81 glaciated mountain group of the Italian Alps (Fig. 1).

82 The La Mare Glacier (World Glacier Inventory code I4L00102517; WGMS 1989) is a
83 3.55 km² valley glacier currently composed of two ice bodies, which have different
84 morphologies and tend to separate (Carturan et al., 2014). In this work, the focus was
85 on the southern ice body, which feeds the main tongue. This 2.1 km² ice body
86 primarily faces north-east, and its surface is rather flat, with the exception of the small
87 remnant of its valley tongue. The elevation ranges from 2660 to 3590 m a.s.l. Mass
88 balance investigations using the direct glaciological method were started on La Mare
89 Glacier in 2003 and detected an average annual mass balance of -0.76 m w.e. y⁻¹
90 during the period from 2003 to 2014 (Carturan, 2016). The mass balance was close
91 to zero in 2013 (-0.06 m w.e.) and was positive for the first time since the beginning
92 of measurements in 2014 (+0.83 m w.e.).

93 The AVDM3 Rock Glacier (Carturan et al., 2015) is an intact, tongue-shaped rock
94 glacier characterized by the presence of two lobes. The 0.058 km² wide Rock Glacier
95 (maximum length of 390 m; maximum width of 240 m) faces south-east and is
96 located at elevations of between 2943 and 3085 m a.s.l. The average slope of the
97 Rock Glacier is 26°, and the slope of the advancing front is 36°. The activity status of
98 the AVDM3 Rock Glacier was assessed via repeated geomorphological field surveys
99 between 2007 and 2014. These surveys revealed the advance of the front of the
100 southern lobe (Carturan, 2010). The general morphology and the elevation of the

101 front also suggest that this rock glacier is active (Seppi et al., 2012), and its
102 permafrost content is further corroborated by spring temperature measurements
103 (Carturan et al., 2015). Moreover, Bertone (2014) provided the first quantification of
104 the surface displacement rates of this rock glacier for 2003 to 2013 using ALS data.

105

106 **3. Methods**

107 **3.1 The ALS data**

108 ALS flights of the study area were available for 17 September 2003, 22 September
109 2013, and 24 September 2014. The technical specifications of the three ALS surveys
110 are reported in Table 1. To avoid errors due to global shifts or rotations between the
111 individual DEMs, the ALS point clouds were automatically co-registered using a
112 version of the ICP algorithm (Chen and Medioni, 1991; Besl and McKay, 1992)
113 tailored to topographic point clouds (Glira et al., 2015). The LiDAR point cloud
114 acquired in 2013 was treated as a reference only for stable areas outside the
115 glaciers, rock glaciers, snow patches, and geomorphologically active areas (e.g.,
116 landslides, river beds, and debris flows). The 2003 and 2014 LiDAR point clouds
117 were iteratively fitted to the reference point cloud by applying an affine
118 transformation. The ICP registration of the point clouds produced z-direction residual
119 values of 0.08 m and 0.11 m for the 2014 and 2003 LiDAR point clouds, respectively.
120 These accuracies can be assumed to be sufficient for calculating the annual
121 elevation changes of the glacier and the decadal displacement rate on the rock
122 glacier.

123 The co-registered point clouds were then converted to DEMs using Natural
124 Neighbours interpolations. A pixel size of 1 x 1 m was produced for the La Mare
125 Glacier, whereas a pixel size of 0.5 x 0.5 m was used for the rock glacier, based on
126 the LiDAR point cloud density (Fig. 2). To evaluate the relative ALS DEM accuracies
127 after the co-registration, the elevation difference errors of the DEMs were calculated
128 for the stable areas. The standard deviation from the 2013 ALS DEM was 0.19 m and
129 0.21 m for the 2014 and 2003 DEM comparisons, respectively.

130

131

132 **3.2 The photogrammetric workflow**

133 **3.2.1 Field surveys**

134 The terrestrial photogrammetric surveys of the La Mare Glacier were conducted on 4
135 September 2013 and 27 September 2014, that is, close to the end of the mass
136 balance year and of ALS flights. The timing of the surveys enabled the calculation of
137 the annual mass balance of the glacier and to compare the results with the ALS-
138 based results. On both days, the sky was clear, with almost no cloud cover.

139 To guarantee a safe and easily repeatable survey of the glacier, the direct access to
140 its surface was avoided and the survey was performed from a rocky ridge on the
141 north side of the glacier (Fig. 5). The elevation of the survey ranged from 3100 to
142 3300 m in 2013 and from 2600 to 3300 m in 2014. The distance from the glacier
143 surface to the camera positions dictated by the topography ranged between 300 and
144 2900 m. To cover the entire glacier surface from these positions, the acquired images
145 were panoramic, which involved taking a series of photographs rotating the camera
146 from each individual camera position. In 2013, seven camera positions were used,
147 and 37 photographs were taken with the camera attached to a small tripod to avoid
148 camera shake. In 2014, the number of camera positions was increased to 21, and
149 177 photos were taken freehand (Fig. 3).

150 Both surveys were performed using a SLR Canon EOS 600D. The camera was
151 equipped with a 25-70 mm zoom lens, which was set to a focal length of 25 mm in
152 2013 and 35 mm in 2014.

153 The terrestrial photogrammetric survey of the AVDM3 Rock Glacier was performed
154 on 27 September 2014. In this survey, 198 images were acquired freehand while
155 walking around and on top of the rock glacier. The survey camera was a CANON
156 EOS 5D full frame SLR camera equipped with a fixed-focal lens of 28 mm. The
157 photographs were acquired and saved in RAW format in both surveys.

158

159 **3.2.2 Data processing**

160 The photogrammetric approach, based on SfM algorithms, can automatically derive
161 the 3D position of an object in images taken in sequence calculating the camera
162 parameters (intrinsic and extrinsic) (Hartley and Zissermann, 2004). Dense image
163 matching algorithms are then used to reconstruct the 3D model of the object as a

164 dense point cloud. Multiple photogrammetric packages implementing SfM and Multi-
165 View Stereo (MVS) algorithms for dense image matching exist, and in this work, the
166 software PhotoScan Pro (AgiSoft LLC. 2010a) was used. Henceforth, the
167 photogrammetric surveys and results are referred to using the acronym SfM-MVS.

168 The photo-based reconstruction workflow is summarized in Fig. 4. The key
169 components of the workflow are 1) acquisition and photograph editing, 2) GCPs
170 identification, image feature detection, matching and 3D scene reproduction (the
171 SfM-MVS steps), 3) point cloud processing, (filtering, subsampling and ICP) and 4)
172 DEM reconstruction.

173 To overcome the significant variability in brightness during the surveys, the RAW
174 images have been edited to adjust the exposure and contrast in order to retrieve
175 information from the overexposed (e.g., snow-covered) areas and underexposed
176 (e.g., shadowed) areas. These editing steps had a positive impact on the number of
177 image features extracted. The edited images were saved in TIFF format and loaded
178 in PhotoScan where non-stationary objects (i.e., clouds and shadows), the sky, and
179 features lying in the distant background have been masked.

180 The camera calibration parameters were calculated using artificial targets prior to the
181 processing of the photogrammetric surveys (pre-calibrated camera). The intrinsic
182 parameters were kept constant during the entire SfM processing given the limits of
183 the camera network geometry and the homogeneous texture of the surveyed terrain.
184 As additional constraint, the GCPs were included into the SfM process to avoid
185 instability in the bundle adjustment solution (Verhoeven et al., 2015). The GCPs were
186 selected as natural features in stable area outside the glacier and rock glacier, and
187 their coordinates were extracted from the 2013 ALS hillshaded DEM. After the SfM
188 step, the geo-referenced dense point cloud was reconstructed by the MVS algorithm,
189 using the 'mild' smoothing filter to preserve as much spatial information as possible
190 (AgiSoft LLC., 2010b).

191 To reduce the noise and outliers generated during the dense matching reconstruction
192 (Bradley et al., 2008; Nilosek et al., 2012), an initial filtering was performed in
193 PhotoScan to manually remove the outliers. Further denoising was applied to the
194 dense point clouds exported from PhotoScan, using a specific tool to treat the point
195 clouds. To obtain a uniform spatial distribution of the points, the photogrammetric
196 point clouds (much denser than the ALS point clouds), were down-sampled to 20 cm
197 for the glacier and 10 cm for the rock glacier. Following the same procedure used for

198 the ALS data, the ICP algorithm (OpalsICP, TU Wien) was applied to co-register the
199 point clouds in the stable area outside the glacier and rock glacier, using the 2013
200 ALS point cloud as a reference. The co-registered point clouds were then converted
201 to DEMs, using the Natural Neighbours interpolation and the pixel sizes of the ALS
202 DEMs (i.e., 1 x 1 m for the glacier and 0.5 x 0.5 m for the rock glacier). The data
203 acquisition settings and processing results of the photogrammetric surveys are
204 summarized in Table 2.

205

206 **3.3 Analyses**

207 The accuracy of the photogrammetric DEMs was assessed calculating the mean, the
208 mean of the absolute values and the standard deviation (σ) of the elevation
209 differences (DEM of Difference, DoD) between SfM-MVS DEMs and ALS DEMs,
210 using the latter as a reference dataset. For both surveyed areas, the primary factors
211 controlling the quality of the photogrammetric results (i.e., camera–object distance,
212 slope and angle of incidence, camera network geometry, surface texture and
213 shadows) were evaluated in terms of DEM accuracy and spatial resolution. The
214 obtained results were compared to the theoretical behaviour of the error as a function
215 of the depth (σ_d), calculated using the following formulation:

$$216 \quad \sigma_d = m_B \cdot \frac{D}{B} \cdot \sigma_i, \quad (1)$$

217 where m_B represents the image scale ($D / \text{focal length}$); D is the depth (camera-object
218 distance); B is the baseline and σ_i is the measured accuracy in the image space.

219 After the accuracy assessments, we investigated the suitability of using the terrestrial
220 photogrammetric surveys to calculate the annual mass balance of the glacier and the
221 surface displacement rates of the rock glacier, comparing the results with those
222 obtained from ALS surveys. The mass balance and elevation changes were
223 calculated differencing multitemporal DEMs.

224 The geodetic mass balance was calculated from the total volume change ΔV (m^3)
225 between two survey dates:

$$226 \quad V = \overline{\Delta z} \cdot A \quad (2)$$

227 where $\overline{\Delta z}$ is the average elevation change between two DEMs over the area A of the
228 glacier. The area-averaged net geodetic mass balance in metres of water equivalent
229 per year (m w.e. y^{-1}) was calculated as:

$$230 \quad \dot{M} = \frac{\Delta V \cdot \rho}{A} \quad (3)$$

231 where ρ is the mean density. The area A of the glacier between the two surveys did
232 not change. The mean density was obtained by a fractional area-weighted mean,
233 assigning 900 kg/m^3 for the ablation area (Huss, 2013) and 530 kg/m^3 for the
234 accumulation area, as directly measured in a snowpit. The resulting weighted mean
235 density was 600 kg/m^3 . In the mass balance calculations, both raw $\overline{\Delta z}$ values and
236 corrected $\overline{\Delta z}$ values were used to account for the mean errors in the stable areas
237 outside the glacier, as reported in Table 3. Other processes like ice fluxes, varying
238 snow density and re-freezing of melt water were assumed to be negligible for the
239 calculation of the annual geodetic mass balance (Zemp et al., 2013).

240 The horizontal surface displacements rates of the AVDM3 rock glacier were
241 estimated by a manual measurement of the displacement of single boulders identified
242 in the hillshaded DEMs. Several points were also located outside the rock glacier to
243 assess the accuracy of the surface velocity determinations. Displacements in the
244 horizontal plane were analysed instead of 3D displacements, which are affected by
245 surface elevation changes (Isaksen et al., 2000).

246

247 **4. Results**

248 **4.1 Accuracy assessment on the area of La Mare Glacier**

249 The mean elevation difference between the SfM-MVS DEM from 4 September 2013
250 (Fig. 5a) and the ALS DEM from 22 September 2013 (Fig. 2b), evaluated in the
251 common stable area outside the glacier, was -0.42 m ($\sigma = 1.72 \text{ m}$). The same
252 calculation between the SfM-MVS DEM from 27 September 2014 (Fig. 5b) and the
253 ALS DEM from 24 September 2014 (Fig. 2a) yielded a mean value of 0.03 m ($\sigma =$
254 0.74 m). In this area, the mean difference between the 2014 and 2013 SfM-MVS
255 DEMs is 0.38 m ($\sigma = 1.73 \text{ m}$), and the mean difference between the respective ALS
256 DEMs is -0.09 m ($\sigma = 0.29 \text{ m}$, Table 3).

257 These results show that the photogrammetric survey conducted in 2014, using a
258 higher number of camera positions and photographs and a slightly longer focal
259 length, provided a significant improvement compared to the survey of 2013. In
260 addition to the higher σ , the 2013 SfM-MVS DEM has a residual average bias of -
261 0.42 m, which must be taken into account in the glacier mass balance calculations.
262 Table 3 presents the same statistics for the area of the glacier. However, given that in
263 2013 the ablation was not negligible between the photogrammetric survey of 4
264 September and the ALS survey of 22 September, the comparison between SfM-MVS
265 and ALS of the same year is meaningful only in 2014, with a mean difference of 0.23
266 m ($\sigma = 0.65$ m). The comparison of the two ALS DEMs of 2014 and 2013 yields a
267 mean difference of 1.30 m for the glacier, attributable to the positive mass balance
268 experienced by the glacier in that time period (+0.83 m w.e., Carturan, 2016).

269 The spatial distribution of the elevation difference between the SfM-MVS and ALS
270 DEMs surveyed at the same times (Fig. 6 and 7) suggests that the most problematic
271 areas for photogrammetric reconstructions are those that are far from the camera
272 positions, steep, and covered by fresh snow. Certain outliers can be observed in
273 steep areas outside the glaciers, even after filtering, but they likely have no influence
274 on the glacier, where the slope is much lower.

275 The factors controlling the quality of the photogrammetric DEMs were investigated in
276 detail using the SfM-MVS DEM from 27 September 2014, which has a higher spatial
277 coverage than that of 2013 and is almost contemporaneous with the ALS DEM from
278 24 September 2014 (which means negligible ablation and accumulation on the
279 glacier).

280 As expected, the standard deviation of elevation differences between the 2014 SfM-
281 MVS and ALS DEMs is proportional to slope but remains lower than 1 m up to 40° on
282 the glacier and up to 60° in the area outside it (Fig. 8). Grouping the data for slope
283 classes of 10 degrees and excluding classes with less than 1000 grid cells, it was
284 possible to calculate a strong correlation between the absolute value of the elevation
285 difference and the slope ($R = 0.86$ both inside and outside the glacier, significant at
286 the 0.05 level). A rapid increase in the error is observed for the highest slope classes,
287 which represent a very small part of the investigated area. For the glacier, only 1% of
288 the area has a slope higher than 40°. The mean elevation difference is around zero
289 for most of the low- and middle-slope classes, with the exception of the 0-10° class
290 inside the glacier, where a mean value of 0.41 m ($\sigma = 0.44$ m) was calculated.

291 Interestingly, the majority of this slope class lies in a flat area of the glacier at 3200-
292 3300 m a.s.l. and is covered by fresh snow, which has poor texture. In addition, this
293 zone has an unfavourable line of sight from the camera positions.

294 The role of the incidence angle between the line of sight of the camera and the
295 photographed object (vector normal to the surface), was investigated by analysing
296 the mean angles calculated from five representative camera locations at different
297 elevations. The analysis was performed for the glacier area, where most of the mean
298 incidence angles ranges between 70° and 90° (75%, Figure 9a). The scatterplot of
299 elevation differences between the 2014 SfM-MVS and ALS DEMs versus the mean
300 incidence angles calculated for every pixel shows no statistically significant
301 relationship ($R = 0.21$). However, by analysing this relationship for classes of
302 incidence angle, and considering the mean of the elevation differences in absolute
303 value and the classes with more than 1000 pixels, yields a correlation coefficient $R =$
304 0.95 (significant at the 0.05 level).

305 Because the redundancy of the observations, that is the number of cameras that
306 views the same points on the glacier, influences the quality of the photogrammetric
307 results, a viewshed analysis was carried out (Fig. 9d). The results show anti-
308 correlation between the absolute value of elevation difference and the number of
309 cameras viewing reconstructed pixels (Fig. 9e), yielding a coefficient of correlation of
310 -0.63 , which is significant at the 0.05 level.

311 The effect of the camera-object distance (i.e., depth, Gómez-Gutiérrez et al., 2014),
312 was evaluated by calculating the mean and standard deviation of the elevation
313 difference between the 2014 SfM-MVS and ALS DEMs, clustering the pixels in 200 m
314 distance classes from a camera position at the centre of the array displayed in Figure
315 4b. The relationship between error and depth is clearer for the glacier area (Fig. 10a),
316 whereas in the surrounding area, the error appears to be more influenced by the
317 variability of the slope angle (Fig. 10b).

318 The theoretical σ_d was calculated using Eq. 1 for each class of distance, considering
319 a mean baseline of 400 m and an accuracy in the image space of 0.40 pixel, which is
320 the reprojection error after bundle adjustment computations. Another quantification of
321 the error as a function of the depth was obtained, for comparison purposes, by
322 multiplying the Ground Sample Distance (GSD) (which increases with depth) by the
323 reprojection error provided by PhotoScan for the Ground Control Points. Figure 10c
324 shows that, on the glacier, the accuracy calculated from the DoD matches quite well

325 the 'theoretical' calculations up to a depth of 1900 m. Beyond this distance, the
326 detected error increases faster than in theory, likely due to the increasing coverage of
327 fresh snow, which affects the image texture and decreases the accuracy.

328 The accuracy of photogrammetric reconstructions for the different substrata was then
329 evaluated. The spatial distribution of each substratum was outlined on the orthophoto
330 exported from PhotoScan. Debris, ice and firn display similar accuracy, with median
331 values of elevation difference between the 2014 SfM-MVS and ALS-based DEMs
332 close to zero and interquartile ranges of the same magnitude. Conversely, the area
333 covered by fresh snow, which is also the area with greater depth, shows prevailing
334 positive differences, a median value of 0.48 m and a much higher standard deviation
335 ($\sigma = 0.82$ m).

336 The texture of the surface also influences the point density distribution and the spatial
337 coverage of the reconstructed area. A lower value of the point density was obtained
338 for fresh snow (4 pts m⁻²). Increasing point densities were obtained for firn, ice and
339 debris (10, 13 and 15 pts m⁻², respectively).

340 The spatial coverage in the fresh snow area was 75%, whereas it was 93% in the
341 rest of the glacier. Excluding the areas not visible from the camera position and
342 occlusions imposed by the topography, the spatial coverage in the fresh snow area
343 was 82% and 98% in the remaining part.

344 The point density is also affected by the depth, elevation and slope (Fig. 12). Due to
345 the GSD, the average point density decreases with depth, which in our case is also
346 proportional to the elevation. On the glacier, the point density decreases more rapidly
347 than in the surrounding area for elevations between 3100 and 3300 m a.s.l., due to
348 the poor texture in this snow-covered flat area. Increasing densities with slope, up to
349 70-80°, are observed and likely result from more favourable incidence angles, which
350 do not however guarantee high accuracy, as noted earlier (Fig. 9). Considering the
351 entire reconstructed surface, the point density was higher in the area surrounding the
352 glacier than on it (12 pts m⁻² vs. 8 pts m⁻², respectively).

353

354 **4.2 Accuracy assessment in the area of the AVDM3 Rock Glacier**

355 The 2014 terrestrial photogrammetric survey of the AVDM3 Rock Glacier provided a
356 good spatial coverage (83%) of high-resolution terrain data (Fig. 13). The spatial
357 distribution of the elevation difference between the contemporaneous SfM-MVS and

358 ALS DEMs shows the existence of areas with both positive and negative values (Fig.
359 14). The average elevation difference is 0.02 m on the rock glacier ($\sigma = 0.17$) and
360 0.05 in the surrounding areas ($\sigma = 0.31$ m, Tab. 5).

361 Similar to the La Mare Glacier area, the accuracy decreases with increasing slope in
362 the rock glacier area. The standard deviation of the average elevation difference
363 between the SfM-MVS and ALS DEMs is less than 0.20 m up to 40°. In the area
364 surrounding the rock glacier, the error increases faster with slope because steep
365 areas coincide with shaded areas and (because the images were acquired in the
366 afternoon) high solar zenith angles. As suggested by Gómez-Gutiérrez et al., (2014),
367 the relationship between the quality of the photogrammetric DEM and the amount of
368 shadowed-lighted areas in the photographs was calculated using a hillshaded model
369 that was calculated by simulating the position of the sun in the sky (azimuth and
370 zenith angles) during the survey. As shown in Figure 16, larger errors occur in
371 shadowed areas and smaller errors in well-lit areas, even if the largest differences in
372 accuracy can be observed outside rather than on the rock glacier.

373

374 **4.3 Glacial and periglacial processes**

375 **4.3.1 Mass balance of La Mare Glacier**

376 Due to abundant solid precipitation during the accumulation season and low ablation
377 rates during the summer (the glacier was snow-covered above ~3000-3100 m a.s.l.),
378 the mass balance of the La Mare Glacier was positive in the 2013-14 hydrological
379 year for the first time since the beginning of measurements in 2003. According to the
380 direct glaciological method, the annual mass balance was +0.83 m w.e. (Carturan,
381 2016).

382 As shown in Table 4, the geodetic mass balance estimates using only ALS data do
383 not differ significantly for either the entire glacier or the sub-areas covered by the
384 photogrammetric surveys of 2013 and 2014 (88% and 93%, respectively). The
385 estimates range between 0.85 and 0.88 m w.e for the raw data and between 0.90
386 and 0.94 m w.e. for the corrected data. The geodetic mass balance calculations
387 using only photogrammetric data yield a raw value of 1.09 m w.e. and a corrected
388 value of 0.87 m w.e. Using the 2014 SfM-MVS, which has a higher quality than the
389 2013 ALS DEM, yields a raw value of 0.98 m w.e. and a corrected value of 1.02 m

390 w.e. Area-averaged estimates of the geodetic mass balance from photogrammetric
391 data are very close to the estimates from ALS data and from the direct method and
392 are closer still if the mean DEM error in the stable areas outside the glacier is
393 subtracted from the raw average elevation differences. The spatial distribution and
394 magnitude of elevation change is also well captured by the terrestrial
395 photogrammetry (Fig. 17 and 18), even if, as already noted in the previous section,
396 problematic areas are present in the upper part of the glacier, which was covered by
397 fresh snow, especially in the 2013 SfM-MVS survey.

398

399 **4.3.2 Surface changes and velocities of the AVDM3 Rock Glacier**

400 The spatial distribution and the mean value of elevation change on the surface of the
401 AVDM3 Rock Glacier were calculated differencing the available SfM-MVS and ALS
402 DEMs. Table 5 shows that, according to the ALS data, there was a prevailing
403 lowering of the surface in the period from 2003 to 2014. Taking into account the
404 average residual bias in the stable area outside the rock glacier, the average
405 lowering rates of the rock glacier surface were 1.5 cm y^{-1} in the period from 2003 to
406 2013, and 2 cm in the year 2013-14. Comparing the SfM-MVS DEM of 2014 with the
407 ALS DEMs of 2013 and 2003 and accounting for the mean bias outside the rock
408 glacier, we obtained slightly higher lowering rates of 2.2 cm y^{-1} from 2003 to 2013
409 and 5 cm from 2013 to 2014. As expected on the basis of the accuracy assessment
410 (Section 4.2), the decadal lowering rates calculated from the SfM-MVS DEM are in
411 closer agreement with those calculated from ALS data than the single-year
412 calculations. The same can be observed for the spatial distribution of the elevation
413 changes (Fig. 19), which shows a prevailing thinning in the upper and middle part of
414 the rock glacier and a thickening of the two advancing lobes. Figure 20 shows that
415 the fastest moving areas in the period from 2003 to 2014 were the two frontal lobes,
416 which also featured the greatest elevation changes. Table 6 shows that the SfM-MVS
417 and ALS data produced very similar surface velocities for the three sub-areas (each
418 with homogeneous displacement) into which the rock glacier can be divided. Outside
419 the rock glacier, the photogrammetric method exhibited a slightly lower accuracy
420 compared to the ALS, but no systematic shift of the different DEMs was found.

421

422 5. Discussion

423 5.1 Data processing and accuracy assessments

424 The results of our terrestrial photogrammetry applications on the La Mare Glacier and
425 on the AVDM3 Rock Glacier demonstrate that it is possible to reliably quantify the
426 investigated glacial and periglacial processes by means of a quick and safe survey
427 that was conducted on a single day using cheap, light and easy-to-use hardware.
428 Moreover, time-consuming and unsafe direct access to the glacier surface was not
429 required.

430 The data processing times were significantly long. For a single operator, the
431 processing time is approximately 10 days. The most labour-intensive and time-
432 consuming tasks were the pre-processing steps i.e., masking of the photos,
433 identification of reference points from the LiDAR DEM and then in the images, and
434 processing of the images (the MVS step is particularly computationally intensive),
435 which is directly related to the resolution and the number of photographs uploaded
436 and the computer performance. Several steps required a certain degree of
437 subjectivity, e.g., the identification of the GCPs. However, due to the high automatism
438 of the image processing, the level of expertise is considerably lower than for LiDAR
439 and traditional photogrammetry.

440 On the La Mare Glacier, the area-averaged estimates of the 2013-14 geodetic mass
441 balance from ALS and photogrammetric data were almost identical (0.91 and 0.87 m
442 w.e., respectively) and close to the mass balance calculated from the direct
443 glaciological method (0.83 m w.e.). The differences are well within the uncertainty of
444 the direct mass balance estimates, which was quantified in 0.26 m w.e. y^{-1} by
445 Carturan (2016). These results confirm that the good results obtained by Piermattei
446 et al., (2015) on the small Montasio Glacier, in the Julian Alps, can also be replicated
447 on larger glaciers with different morphologies and characteristics.

448 Because the AVDM3 Rock Glacier exhibited quite slow annual deformation and
449 creep, we were able to calculate reliable displacement rates and area-averaged
450 surface elevation changes only on a multi-year (in our case, decadal) time scale. This
451 result confirms the findings of Gómez-Gutiérrez et al. (2014), who applied a similar
452 method to the Corral del Veleta Rock Glacier in the Sierra Nevada (Spain).

453 Our results are promising, despite the limitations of the adopted method, which
454 include i) the location of GCPs on natural targets outside the investigated glacier/rock

455 glacier, ii) the presence of areas with deep shadows and changes in the light during
456 the survey, iii) the presence of fresh snow in the upper and middle part of the glacier,
457 and iv) the high camera-object distance in the glacier application.

458 In general terms, the photo-based accuracy is related to the image feature extraction,
459 feature matching (in both the SfM and MVS steps), and scale definition (Bemis et al.,
460 2014). A low accuracy in these steps, caused for example by poor camera network
461 geometry, can generate model distortion and reduce the ability to identify unique
462 corresponding features in overlapping images (Wackrow and Chandler, 2011;
463 Dall'Asta et al., 2015, Favalli et al., 2012; James and Robson, 2012; 2014;
464 Hosseinaveh et al, 2014; Micheletti et al., 2014; Nocerino et al., 2014). In our case
465 studies, among the various aspects analysed, the spatial variability of the accuracy of
466 the photogrammetric DEMs is related to the camera-object distance, the presence of
467 fresh snow with low contrast, the changing illumination during the survey and the
468 occurrence of shadows. The increasing error with increasing terrain slope suggests
469 the persistence of a small shift in the reconstructed DEMs. This shift, however does
470 not affect the areal estimates of mass balance and elevation change, given that the
471 vast majority of the glacier and rock glacier areas feature small or moderate slope
472 angles. For both the glacier and the rock glacier, the spatial coverage of the
473 reconstructed areas was not complete. In the glacier surveys, the problematic areas
474 were those visible from a low number of camera positions and those covered by fresh
475 snow and far from the viewpoints. In the rock glacier, certain areas were not
476 reconstructed due to the rock glacier's complex morphology and in particular to the
477 presence of ridges, furrows and counterslopes.

478

479 5.2 Possible improvements of the SfM-MVS approach

480 The accuracy assessments confirm that the ALS data still provide results with
481 somewhat higher accuracies (Tabs. 3 and 5, Figs. 6 and 14) but with much higher
482 costs and demanding logistics than the SfM-MVS approach. However, the SfM-MVS
483 method has the potential to provide a significantly higher spatial resolution (Debella-
484 Gilo and Kaab, 2011; Piermattei et al., 2015) and temporal resolution due to its
485 significantly lower costs. Moreover, the photogrammetric reconstructions still have
486 room for improvement, as demonstrated by the better results achieved from the 2014
487 survey of the glacier area compared to those from 2013. This improvement resulted
488 from a higher number of photographs and improved camera network geometry.

489 Many of the limitations described above can be overcome by introducing
490 modifications to the terrestrial photogrammetric survey strategy. For the rock glacier
491 survey, shorter baselines are recommended to ensure greater spatial coverage, high
492 image similarity and good matching performance (Wenzel et al., 2013). GCPs, for
493 example, could be placed on the surface of the glaciers and rock glaciers to reduce
494 the model distortions (Bemis et al., 2014) and generate surveys with much higher
495 accuracies via, for example, the use of dGPS (Dall'Asta et al., 2015).

496 The use of UAVs could solve the problem of excessive camera-object distances and
497 the issue of missing areas due to inaccessibility. However, these alternatives imply
498 increased costs, more troublesome logistics, greater expertise, and ultimately longer
499 survey times. In addition, they also require directly accessing unsafe or difficult to
500 reach areas, both to place targets and to move UAVs among study areas that exceed
501 their operational range (Bühler et al., 2014). Therefore, the best balance must be
502 found between simplicity, safety, costs and accuracy for each photogrammetric
503 application based on the final objectives and on the available human and economic
504 resources.

505

506 **6. Conclusions**

507 In this paper, we investigated the applicability of the SfM-MVS approach for
508 monitoring glacial and periglacial processes in a catchment of the Ortles-Cevedale
509 Group (Eastern Italian Alps), validating our results using ALS DEMs as benchmarks.
510 The ground surveys were conducted on foot and were intentionally planned to be as
511 quick and easy as possible. The 2.1 km² La Mare Glacier and the neighbouring
512 AVDM3 Rock Glacier were surveyed in one day using only a consumer-grade SLR
513 camera without the setup of artificial targets.

514 The accuracy of the photogrammetric DEMs, evaluated as the mean and standard
515 deviation of the elevation difference in a stable area between the SfM-MVS DEM and
516 the reference ALS DEM, was $-0.42 \text{ m} \pm 1.72 \text{ m}$ and $0.03 \text{ m} \pm 0.74 \text{ m}$ for the 2013 and
517 2014 surveys, respectively. The SfM-MVS DEM accuracy of the reconstructed rock
518 glacier surface acquired in 2014 was estimated to be $0.02 \text{ m} \pm 0.17 \text{ m}$.

519 The SfM-MVS geodetic mass balance estimates for the La Mare Glacier were in
520 good agreement with the calculations from the contemporary ALS data and with the
521 results of the direct glaciological method, confirming a positive mass balance of

522 approximately 0.9 m w.e. in the 2013-14 hydrological year. In the rock glacier, the
523 survey produced a good spatial coverage of the photogrammetric DEM and a reliable
524 calculation of the multi-year surface changes and displacement rates. For rock
525 glacier applications, particularly for slow-mowing ones such as AVDM3, single-year
526 assessments of elevation change and surface velocities require the setup of artificial
527 targets and GCPs to obtain the accuracy required to detect such slow processes.
528 The simplicity of the ground surveys and the physical characteristics of the analysed
529 alpine terrain were the main factors influencing the tested approach. In particular, we
530 refer to the use of natural targets as GCPs, the occurrence of shadowed areas and
531 lighting changes during the surveys, the presence of fresh snow in the upper part of
532 the glacier (which reduced the contrast), and the sub-optimal camera network
533 geometry and long camera-object distances imposed by the morphology and
534 accessibility of the study area. In consideration of the factors that spatially control the
535 accuracy of the SfM-MVS DEMs, there remains room for significant improvements,
536 e.g., using aerial platform and/or placing artificial targets surveyed by dGPS. Further
537 research is therefore needed to i) find technical solutions to overcome the major
538 limitations of the SfM-MVS approach in such remote areas and ii) achieve the optimal
539 balance between the simplicity and low cost of this approach and the accuracy
540 required for each specific application.

541

542 **Acknowledgments**

543 This study was funded by the Italian MIUR Project (PRIN 2010-11): 'Response of
544 morphoclimatic system dynamics to global changes and related geomorphological
545 hazards' (local and national coordinators G. Dalla Fontana and C. Baroni). The
546 authors would like to thank Philipp Glira from the TU of Wien for his precious
547 contribution to the LiDAR data processing. The comments and suggestions from
548 Susan Conway, Álvaro Gómez-Gutiérrez and an anonymous Reviewer have been
549 useful for the improvement of the manuscript.

550

551

552

553 **References**

554 AgiSoft LL C: AgiSoft PhotoScan Professional Edition. Version 1.1.2, available at:
555 <http://www.agisoft.ru/products/photoscan/> (last access: 18 January 2015), 2010a.

556 AgiSoft LL C: AgiSoft PhotoScan User-manuals Version 1.0, available at:
557 http://www.agisoft.com/pdf/photoscan-pro_1_1_en.pdf (last access: 15 May 2015),
558 2010b.

559 Bemis, S., Micklethwaite, S., and Turner, D.: Ground-based and UAV-Based
560 photogrammetry: a multi-scale, high-resolution mapping tool for Structural Geology
561 and Paleoseismology. *J Struct Geol.*, 69, 163–178, doi:10.1016/j.jsg.2014.10.007,
562 2014.

563 Bertone, A.: Misure di spostamento dei rock glacier con l'uso di feature tracking
564 applicato a DTM multitemporali, BSc Thesis, Department of Earth and Environmental
565 Sciences, University of Pavia, Pavia, Italy, 63 pp., 2014.

566 Besl, P. J. and McKay, N. D.: Method for registration of 3-D shapes, in: Proceedings
567 of the International Society for Optics and Photonics IEEE Transactions on Pattern
568 Analysis and Machine Intelligence, 1611, 586–606, 1992.

569 Bradley, D., Boubekeur, T., and Heidrich, W.: Accurate multi-view reconstruction
570 using robust binocular stereo and surface meshing, in: IEEE Conference on
571 Computer Vision and Pattern Recognition, Anchorage, AK, USA, 1–8, 2008.

572 Bühler, Y., Marty, M., Egli, L., Veitinger, J., Jonas, T., Thee, P., and Ginzler, C.:
573 Spatially continuous mapping of snow depth in high alpine catchments using digital
574 photogrammetry, *The Cryosphere Discuss.*, 8, 3297–3333, doi:10.5194/tcd-8-3297-
575 2014, 2014.

576 Carturan, L.: Climate change effects on the cryosphere and hydrology of a high-
577 altitude watershed, PhD thesis, Department of Land, Environment, Agriculture and
578 Forestry, University of Padova, Padova, Italy, 2010.

579 Carturan, L.: Replacing monitored glaciers undergoing extinction: a new
580 measurement series on La Mare Glacier (Ortles-Cevedale, Italy), *J. Glaciol.*, in
581 review, 2016.

582 Carturan, L., Cazorzi, F., and Dalla Fontana, G.: Enhanced estimation of glacier
583 mass balance in unsampled areas by means of topographic data, *Ann. Glaciol.*, 50,
584 37–46, 2009.

585 Carturan, L., Baldassi, G., Bondesan, A., Calligaro, S., Carton, A., Cazorzi, F., Dalla
586 Fontana, G., Francese, R., Guarnieri, A., Milan, N., Moro, D., Tarolli, P.: Current
587 behavior and dynamics of the lowermost Italian glacier (Montasio Occidentale, Julian
588 Alps), *Geografiska Annaler: Series A, Physical Geography*, 95, 79–96, 2013.

589 Carturan, L., Baroni, C., Carton, A., Cazorzi, F., Fontana, G. D., Delpero, C., and
590 Zanoner, T.: Reconstructing Fluctuations of La Mare Glacier (Eastern Italian Alps) in
591 the Late Holocene: new Evidence for a Little Ice Age Maximum Around 1600 AD.
592 *Geografiska Annaler: Series A, Physical Geography*, 96, 287–306, 2014.

593 Carturan, L., Zuecco, G., Seppi, R., Zanoner, Z., Borga, M., Carton, A., and Dalla
594 Fontana, G.: Catchment-scale permafrost mapping using spring water
595 characteristics, *Permafrost Periglac.*, in press, doi: 10.1002/ppp.1875, 2015.

596 Chen, Y. and Medioni, G.: Object modeling by registration of multiple range images,
597 in: *Proceedings, IEEE International Conference on Robotics and Automation*, 9–11
598 April, Sacramento, CA, USA, 10, 145–155, 1991.

599 Dall’Asta, E., Delaloye, R., Diotri, F., Forlani, G., Fornari, M., Morra di Cella, U.,
600 Pogliotti, P., Roncella, R., Santise, M.: Use of UAS in a high mountain landscape: the
601 case of gran sommetta rock glacier (AO), *The International Archives of the*
602 *Photogrammetry, Remote Sensing and Spatial Information Sciences*, Volume XL-
603 3/W3, 391–397, 2015a.

604 Debella-Gilo, M. and Käab, A.: Sub-pixel precision image matching for measuring
605 surface displacements on mass movements using normalized cross-correlation.
606 *Remote Sens. Environ.*, 115, 130–142, 2011.

607 Favalli, M., Fornaciai, A., Isola, I., Tarquini, S., and Nannipieri, L.: Multiview 3D
608 reconstruction in geosciences, *Comput. Geosci.*, 44, 168–176, 2012.

609 Gauthier, D., Conlan, M., and Jamieson, B.: Photogrammetry of fracture lines and
610 avalanche terrain: potential applications to research and hazard mitigation projects,

611 Proceedings, International Snow Science Workshop, Banff, 29 September–3 October
612 2014, 109–115, 2014.

613 Glira, P., Pfeifer, N., Briese, C., Ressler, C.: A correspondence framework for ALS strip
614 adjustments based on variants of the ICP algorithm, *Photogramm. Fernerkun.*, 4,
615 275–289, doi:10.1127/pfg/2015/0270, 2015.

616 Gómez-Gutiérrez, Á., de Sanjosé-Blasco, J. J., de Matías-Bejarano, J., and
617 Berenguer-Sempere, F.: Comparing two photo-reconstruction methods to produce
618 high density point clouds and DEMs in the Corral del Veleta Rock Glacier (Sierra
619 Nevada, Spain), *Remote Sensing*, 6, 5407–5427, 2014.

620 Gómez-Gutiérrez, Á., de Sanjosé-Blasco, J. J., Lozano-Parra, J., Berenguer-
621 Sempere, F., and de Matías-Bejarano, J.: Does HDR pre-processing improve the
622 accuracy of 3D models obtained by means of two conventional SfM-MVS software
623 packages? The case of the Corral del Veleta Rock Glacier, *Remote Sensing*, 7,
624 10269–10294, 2015.

625 Hartley, R. and Zisserman, A.: *Multiple View Geometry*, In *Computer Vision*,
626 Cambridge University Press, Cambridge, UK, 2003.

627 Haeberli, W.: Creep of mountain permafrost: internal structure and flow of alpine rock
628 glaciers, *Mitteilungen der Versuchsanstalt für Wasserbau, Hydrologie und Glaziologie*
629 *der ETH Zurich*, 77, 5–142, 1985.

630 Hosseiniveh, A., Sargeant, B., Erfani, T., Robson, S., Shortis, M., Hess, M., and
631 Boehm, J.: Towards fully automatic reliable 3D acquisition: from designing imaging
632 network to a complete and accurate point cloud, *Robotics and Autonomous Systems*,
633 62, 1197–1207, 2014.

634 Huss, M.: Density assumptions for converting geodetic glacier volume change to
635 mass change, *The Cryosphere*, 7, 877-887, doi:10.5194/tc-7-877-2013, 2013.

636 Immerzeel, W. W., Kraaijenbrink, P. D. A., Shea, J. M., Shrestha, A. B., Pellicciotti,
637 F., Bierkens, M. F. P., and De Jong, S. M.: High-resolution monitoring of Himalayan
638 glacier dynamics using unmanned aerial vehicles, *Remote Sens. Environ.*, 150, 93–
639 103, 2014.

640 Isaksen, K., Ødegård, R. S., Eiken, T., and Sollid, J. L.: Composition, flow and
641 development of two tongue-shaped rock glaciers in the permafrost of Svalbard.
642 *Permafrost and Periglacial Processes*, 11, 241-257, 2000.

643 James, M. R. and Robson, S.: Straightforward reconstruction of 3D surfaces and
644 topography with a camera: accuracy and geoscience application, *J. Geophys. Res.-*
645 *Earth*, 117, F03017, doi:10.1029/2011JF002289, 2012.

646 James, M. R. and Robson, S.: Mitigating systematic error in topographic models
647 derived from UAV and ground-based image networks, *Earth Surf. Proc. Land.* 39,
648 1413–1420, doi:10.1002/esp.3609, 2014.

649 Kääb, A.: Monitoring high-mountain terrain deformation from repeated air-and
650 spaceborne optical data: examples using digital aerial imagery and ASTER data.
651 *ISPRS Journal of Photogrammetry and remote sensing*, 57, 39–52, 2002.

652 Kääb, A.: Remote Sensing of Mountain Glaciers and Permafrost Creep. Research
653 Perspectives from Earth Observation Technologies and Geoinformatics,
654 *Schriftenreihe Physische Geographie, Glaziologie und Geomorphodynamik*, 48,
655 University of Zurich, Zurich, Switzerland, 2005.

656 Kääb, A., Kaufmann, V., Ladstädter, R., and Eiken, T.: Rock glacier dynamics:
657 implications from high-resolution measurements of surface velocity fields, in: Eighth
658 International Conference on Permafrost, 21–25 July 2003, Zurich, Switzerland, Vol.
659 1, 501–506, 2003.

660 Kääb, A., Girod, L., and Berthling, I.: Surface kinematics of periglacial sorted circles
661 using structure-from-motion technology, *The Cryosphere*, 8, 1041–1056,
662 doi:10.5194/tc-8-1041-2014, 2014.

663 Micheletti, N., Chandler, J. H., and Lane, S. N.: Investigating the geomorphological
664 potential of freely available and accessible Structure-from-Motion photogrammetry
665 using a smartphone, *Earth Surf. Proc. Land.*, 40, 473–486, doi:10.1002/esp.3648,
666 2014.

667 Nilosek, D., Sun, S., and Salvaggio, C.: Geo-accurate model extraction from three-
668 dimensional image-derived point clouds, in: *Proceedings of SPIE, Algorithms and*

669 Technologies for Multispectral, Hyperspectral, and Ultraspectral Imagery XVIII, 23
670 April 2012, Baltimore, MD, USA, 8390, 83900J, doi:10.1117/12.919148, 2012.

671 Nocerino, E., Menna, F., and Remondino, F.: Accuracy of typical photogrammetric
672 networks in cultural heritage 3D modeling projects, *ISPRS-International Archives of*
673 *the Photogrammetry, Remote Sensing and Spatial Information Sciences*, 1, 465–472,
674 2014.

675 Piermattei, L., Carturan, L., and Guarnieri, A.: Use of terrestrial photogrammetry
676 based on structure from motion for mass balance estimation of a small glacier in the
677 Italian Alps, *Earth Surf. Proc. Land.*, 40, 1791–1802, doi:10.1002/esp.3756, 2015.

678 Ryan, J. C., Hubbard, A. L., Box, J. E., Todd, J., Christoffersen, P., Carr, J. R., Holt,
679 T. O., and Snooke, N.: UAV photogrammetry and structure from motion to assess
680 calving dynamics at Store Glacier, a large outlet draining the Greenland ice sheet,
681 *The Cryosphere*, 9, 1–11, doi:10.5194/tc-9-1-2015, 2015.

682 Roer, I. and Nyenhuis, M.: Rockglacier activity studies on a regional scale:
683 comparison of geomorphological mapping and photogrammetric monitoring, *Earth*
684 *Surf. Proc. Land.*, 32, 1747–1758, 2007.

685 Seppi, R., Carton, A., Zumiani, M., Dall’Amico, M., Zampedri, G., and Rigon, R.:
686 Inventory, distribution and topographic features of rock glaciers in the southern region
687 of the Eastern Italian Alps (Trentino). *Geografia Fisica e Dinamica Quaternaria* 35,
688 185–197, doi:10.4461/GFDQ.2012.35.17, 2012.

689 Solbø, S. and Storvold, R.: Mapping svalbard glaciers with the cryowing uas, *ISPRS*
690 *International Archives of the Photogrammetry, Remote Sensing and Spatial*
691 *Information Sciences*, XL-1/W2, 373–377, 2013.

692 Tonkin, T. N., Midgley, N. G., Graham, D. J., and Labadz, J. C.: The potential of
693 small unmanned aircraft systems and structure-from-motion for topographic surveys:
694 a test of emerging integrated approaches at Cwm Idwal, North Wales,
695 *Geomorphology*, 226, 35–43, 2014.

696 Tseng, C.-M., Lin, C. W., Dalla Fontana, G., Tarolli, P.: The topographic signature of
697 a Major Typhoon, *Earth Surf. Proc. Land.*, 40, 1129–1136, 2015.

698 Verhoeven, G., Karel, W., 'tuhac, S., Doneus, M., Trinks, I., and Pfeifer, N.: Mind your
699 grey tones – examining the influence of decolourization methods on interest point
700 extraction and matching for architectural image-based modelling, in: 3D-Arch 2015–
701 3D Virtual Reconstruction and Visualization of Complex Architectures (ISPRS WG
702 V/4, CIPA), 25–27 February 2015, Vol. 40, ISPRS, Avila, Spain, 307–314, 2015.

703 Wackrow, R. and Chandler, J.: Minimising systematic error surfaces in digital
704 elevation models using oblique convergent imagery, *Photogramm. Rec.*, 26, 16–31,
705 2011.

706 Wenzel, K., Rothermel, M., Fritsch, D., and Haala, N.: Image acquisition and model
707 selection for multi-view stereo, *Int. Arch. Photogramm. Remote Sens. Spatial Inf. Sci.*,
708 251–258, 2013.

709 Whitehead, K., Moorman, B. J., and Hugenholtz, C. H.: Brief Communication: Low-
710 cost, ondemand aerial photogrammetry for glaciological measurement, *The*
711 *Cryosphere*, 7, 1879–1884, doi:10.5194/tc-7-1879-2013, 2013.

712 Zemp, M., Thibert, E., Huss, M., Stumm, D., Denby, C. R., Nuth, C., Nussbaumer, S.
713 U., Moholdt, G., Mercer, A., Mayer, C., Joerg, P. C., Jansson, P., Hynek, B., Fischer,
714 A., Escher-Vetter, H., Elvehøy, H., and Andreassen, L. M.: Reanalysing glacier mass
715 balance measurement series. *The Cryosphere*, 7, 1227-1245, doi:10.5194/tc-7-1227-
716 2013, 2013.

717

718

719

720

721

722

723

724

725

726 **Table 1.** Date and main parameters of available LiDAR data.

Date	Aircraft	Laser scanner model	Laser scanner rate	Max. scan angle	Scan frequency	Point density [pts·m ⁻²]
24 Sept. 2014	Elicopter AS350 B3	Optech ALTM GEMINI (04SEN164)	100 kHz	46°	34 Hz	5.1
22 Sept. 2013	Cessna 404 D-IDOS	ALTM 3100	70,000 Hz	±25°	32 Hz	0.9
17 Sept. 2003	—	—	—	—	—	0.5

727

728 **Table 2.** Data acquisition settings and processing results of the photogrammetric
 729 surveys for both case studies. The GCPs error is the average transformation
 730 residuals error [m] and root mean square reprojection error for the GCPs [pix] during
 731 the bundle adjustment computation. The image quality represents the downsized of
 732 the images resolution during the dense matching computation. “Ultra high” means full
 733 resolution, “High” a downsized of 50% before the image matching processing. The
 734 ground sample distance (GSD) is the average pixel size on the ground. The standard
 735 deviation of ICP registration is reported in the table.

	La Mare glacier		Rock glacier
	4 September 2013	27 September 2014	27 September 2014
<i>Input data</i>			
Camera type	Nikon 600D	Nikon 600D	Canon 5D Mark III
Focal Length	25 mm	35 mm	28 mm
Image size	5184 x 3456 pix	5184 x 3456 pix	5760 x 3840 pix
N° Images	37	177	198
<i>Processing data</i>			
Reprojection error	0.43 pix (1.76 max)	0.40 pix (3.75 max)	0.38 pix (1.20 max)
GCPs error	1.52 m 1.48 pix	1.14 m 1.96 pix	0.62 m 1.86 pix
Image quality	Ultra high	High	High
Mean GSD	0.16 m/pix	0.22 m/pix	0.064 m/pix
Dense point cloud	49,844,094 pts	55,114,074 pts	56,171,705 pts
Point density	37 pts m ⁻²	20 pts m ⁻²	244 pts m ⁻²
<i>Post-processing data</i>			
Filtered point cloud /subsampled	15,617,342 pts (sampled 0.20 m)	24,226,221 pts (sampled 0.20 m)	4,517,143 pts (sampled 0.10 m)
Point density	8 pts m ⁻²	9 pts m ⁻²	21 pts m ⁻²
ICP transformation	0.14 m	0.15 m	0.10 m

736

737

738

739 **Table 3.** Results of comparisons between SfM-MVS-based DEMs vs. ALS-based
 740 DEMs in the common area and for the bare-ground stable area and glacier.

Elevation differences [m] cell size 1 m x 1 m									
DEMs	Common SfM-MVS bare-ground area				Common SfM-MVS glacier area				
	<i>Min</i>	<i>Max</i>	<i>Mean</i>	σ	<i>Min</i>	<i>Max</i>	<i>Mean</i>	σ	
SfM-MVS - ALS 2013 2013	-19.59	33.61	-0.42	1.72	-9.91	12.04	-0.13	0.78	
SfM-MVS - ALS 2014 2014	-18.48	22.42	0.03	0.74	-18.17	11.41	0.23	0.65	
SfM-MVS - SfM-MVS 2014 2013	-33.12	14.19	0.38	1.73	-12.44	12.33	1.58	1.42	
ALS 2014 - ALS 2013	-15.38	10.81	-0.09	0.29	-14.61	7.37	1.30	0.97	

741

742 **Table 4.** Mass balance calculations on La Mare Glaciers using different combinations
 743 of SfM-MVS and ALS DEMs.

Mass balance estimation									
DEMs cell size 10 m	Spatial coverage [m ²]	Average elevation		Volume change		Mass balance			
		changes [m]		[m ³]		[m w.e]			
		<i>Raw</i>	<i>Corrected</i>	<i>Raw</i>	<i>Corrected</i>	<i>Raw</i>	<i>Corrected</i>		
SfM-MVS - SfM-MVS 2014 2013	1,834,800 (~88%)	1.81	1.45	3,320,988	2,660,460	1.09	0.87		
ALS 2014 - ALS 2013		1.47	1.56	2,697,156	2,862,288	0.88	0.94		
SfM-MVS - ALS 2013 2014	1,938,700 (~93%)	1.64	1.70	3,179,468	3,295,790	0.98	1.02		
ALS 2014 - ALS 2013		1.41	1.50	2,733,567	2,908,050	0.85	0.90		
ALS 2014 - ALS 2013	2,072,700 (entire glacier)	1.43	1.52	2,963,961	3,150,504	0.86	0.91		

744

745

746

747

748

749

750

751

752

753

754

755 **Table 5.** Statistics of elevation changes in the rock glacier and in bare ground stable
 756 area off rock glacier from September 2014 to September 2013 and September 2003
 757 in the ALS reconstructed area and in the common ALS and SfM-MVS coverage area.

Data		Elevation changes [m]							
		ALS Reconstructed area				SfM-MVS Reconstructed area			
		Stable area		Rock glacier		Stable area		Rock glacier	
<i>Mean</i>	σ	<i>Mean</i>	σ	<i>Mean</i>	σ	<i>Mean</i>	σ		
SfM-MVS 2014	- ALS 2014	—	—	—	—	0.05	0.31	0.02	0.17
SfM-MVS 2014	- ALS 2013	—	—	—	—	0.01	0.33	-0.04	0.18
ALS 2014	- ALS 2013	-0.05	0.19	-0.07	0.12	-0.05	0.20	-0.07	0.12
SfM-MVS 2014	- ALS 2003	—	—	—	—	0.06	0.33	-0.16	0.49
ALS 2014	- ALS 2003	-0.01	0.22	-0.18	0.46	-0.00	0.21	-0.18	0.47
ALS 2013	- ALS 2003	0.04	0.21	-0.11	0.41	—	—	—	—

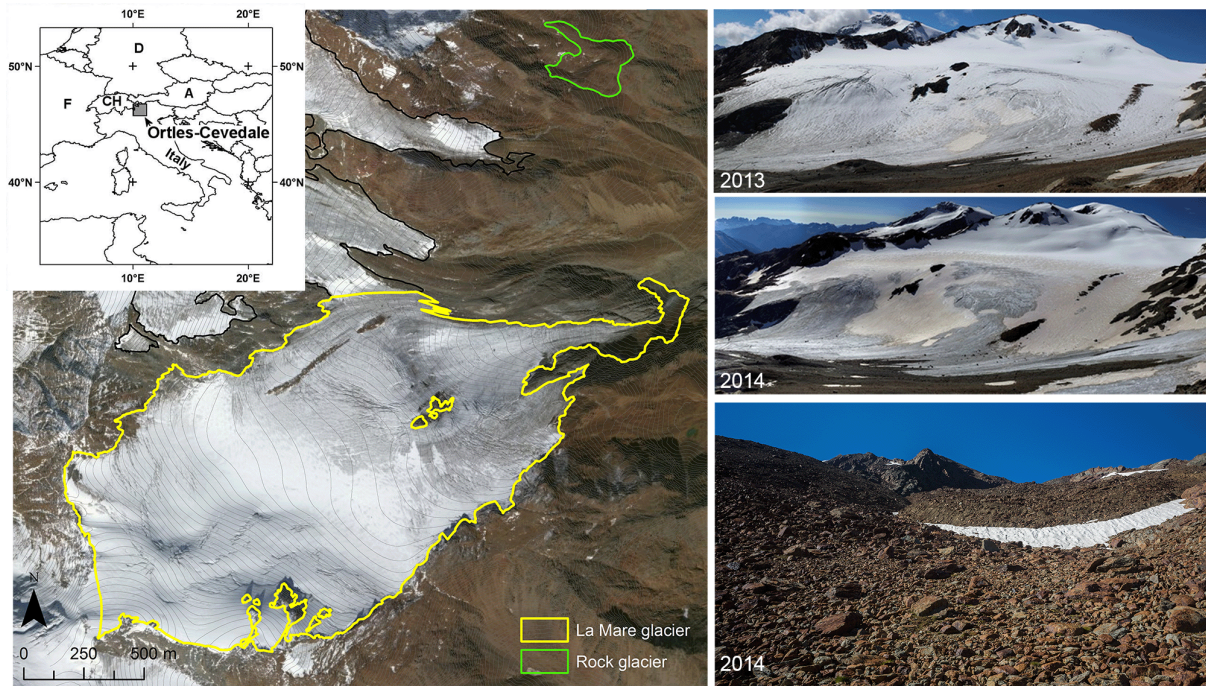
758

759 **Table 6.** Velocity statistics in three distinct areas of the rock glacier and in stable area
 760 outside the rock glacier evaluated comparing the 2003 and 2014 ALS DEMs and the
 761 photogrammetric DEM for the 2014 survey epoch.

Horizontal movements between 2003 and 2014 [cm yr ⁻¹]										
	ALS 2003 - ALS 2014					ALS 2003 - SfM-MVS 2014				
	<i>No. points</i>	<i>Min</i>	<i>Max</i>	<i>Mean</i>	σ	<i>No. points</i>	<i>Min</i>	<i>Max</i>	<i>Mean</i>	σ
Area 1	41	7.3	43.3	26.8	8.9	36	6.8	47.5	26.3	10.3
Area 2	13	4.4	27.4	18.9	7.0	11	9.0	27.9	18.1	6.4
Area 3	26	4.5	16.5	9.4	4.0	24	4.5	18.2	9.0	4.1
Off rock glacier	65	0.0	10.7	3.6	3.1	23	0.0	13.6	5.3	4.2

762

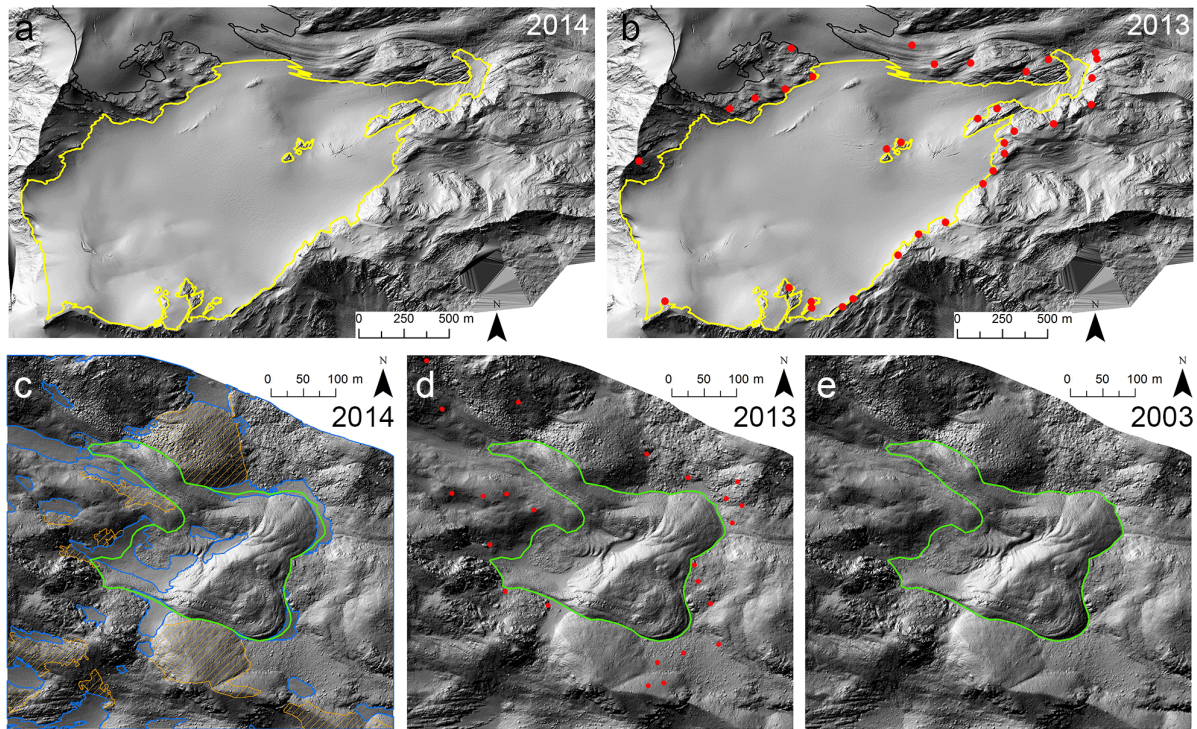
763



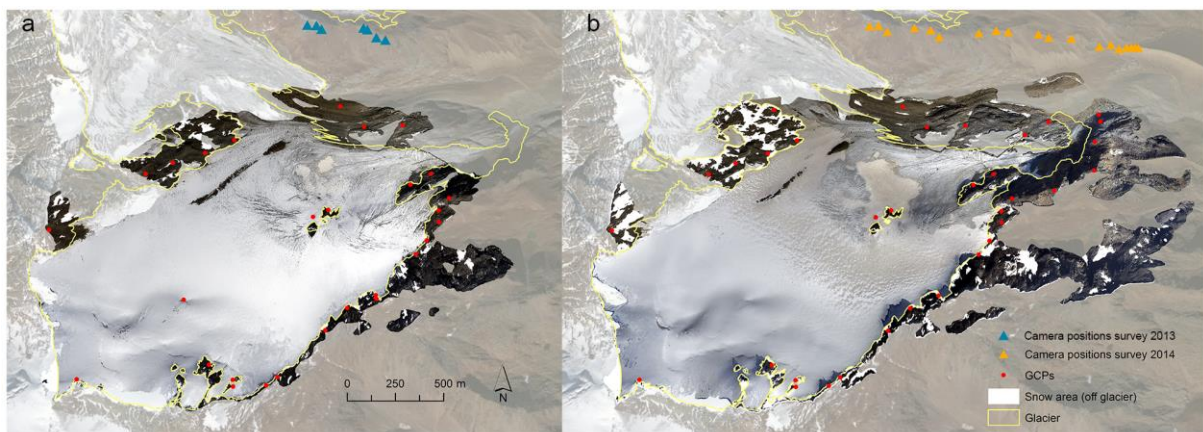
764

765 **Figure 1.** Geographic setting of study areas. Panorama view of the La Mare Glacier
766 from the same camera position on 4 September 2013 and 27 September 2014. The
767 lower right photograph shows the front of the meridional lobe of the AVDM3 Rock
768 Glacier, which was surveyed on 27 September 2014.

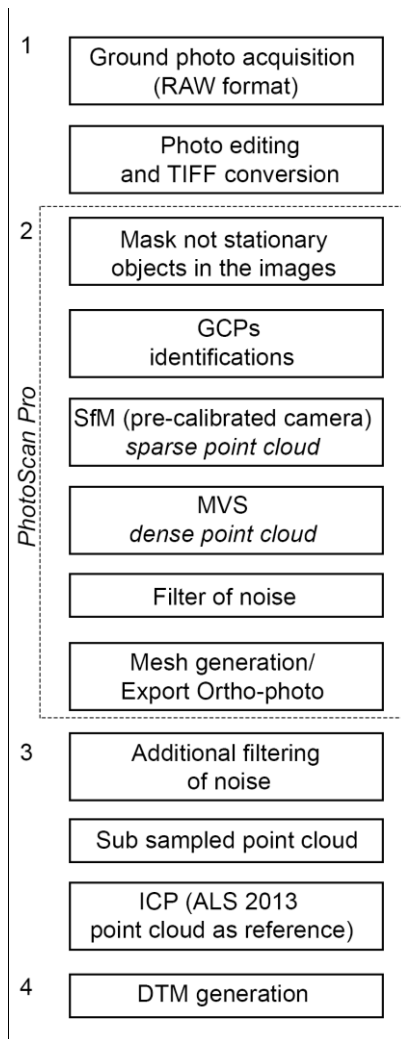
769



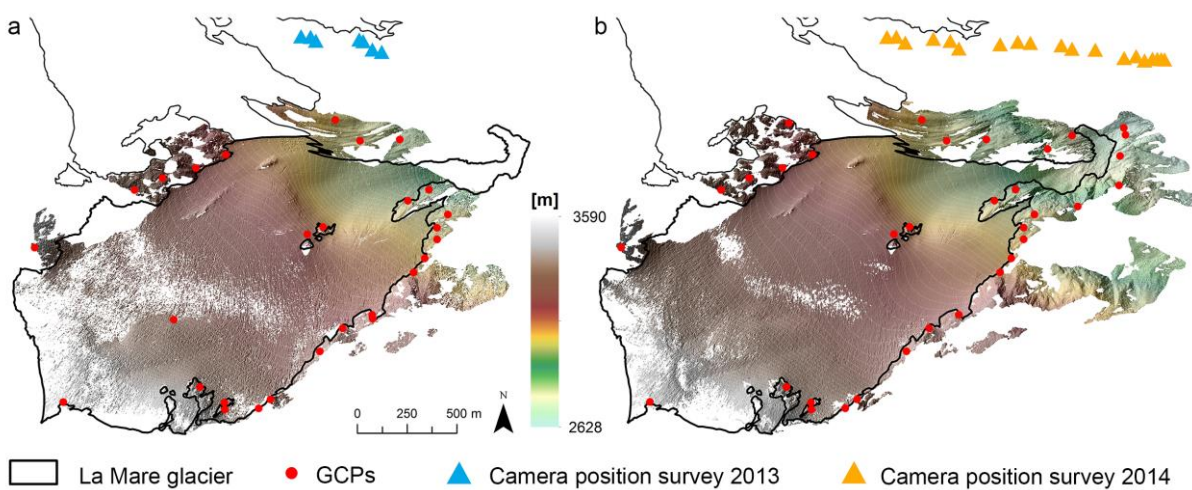
770 ● Ground Control Points □ La Mare glacier □ Rock glacier □ Snow 2014 ▨ Active areas off rock glacier
 771 **Figure 2.** ALS shade DEMs of la Mare glacier acquired on **(a)** September 24, 2014
 772 and **(b)** September 21, 2013. The ALS DEMs of rock glacier acquired on **(c)** 2014,
 773 **(d)** 2013 and **(e)** 2003. The red dots represent the selected GCPs in 2013 DEM used
 774 in the photogrammetric approach. The snow accumulation areas and
 775 geomorphologically-active areas outside the rock glacier were excluded during the
 776 ICP computation between 2013 and 2003, 2014 ALS point cloud.



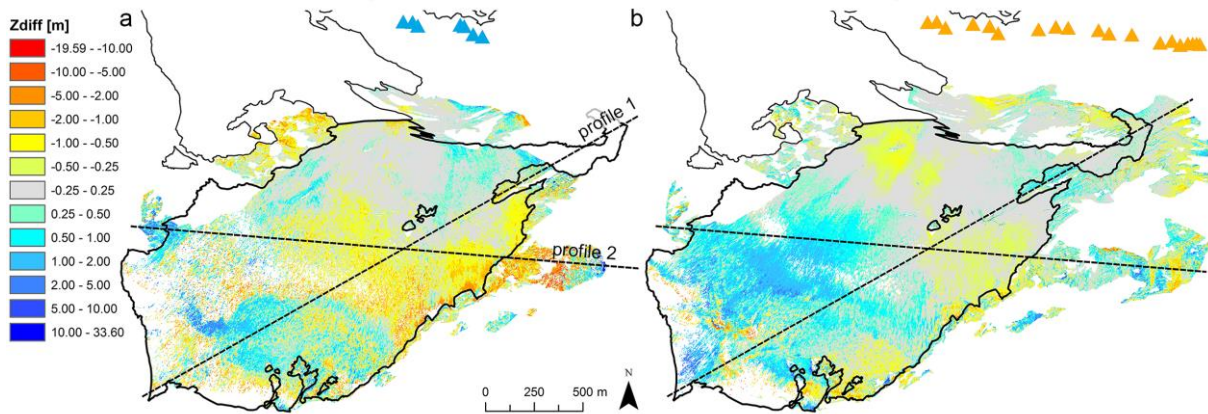
777
 778 **Figure 3.** Orthophoto-images of SfM-MVS 3D model of La Mare glacier surveyed on
 779 **(a)** 4 September 2013 and **(b)** 27 September 2014. The white areas in the ortho-
 780 images represent the snow-covered area in the rock stable area. The red dots
 781 outside the glacier area are the GCPs and the triangles identified the camera
 782 locations.



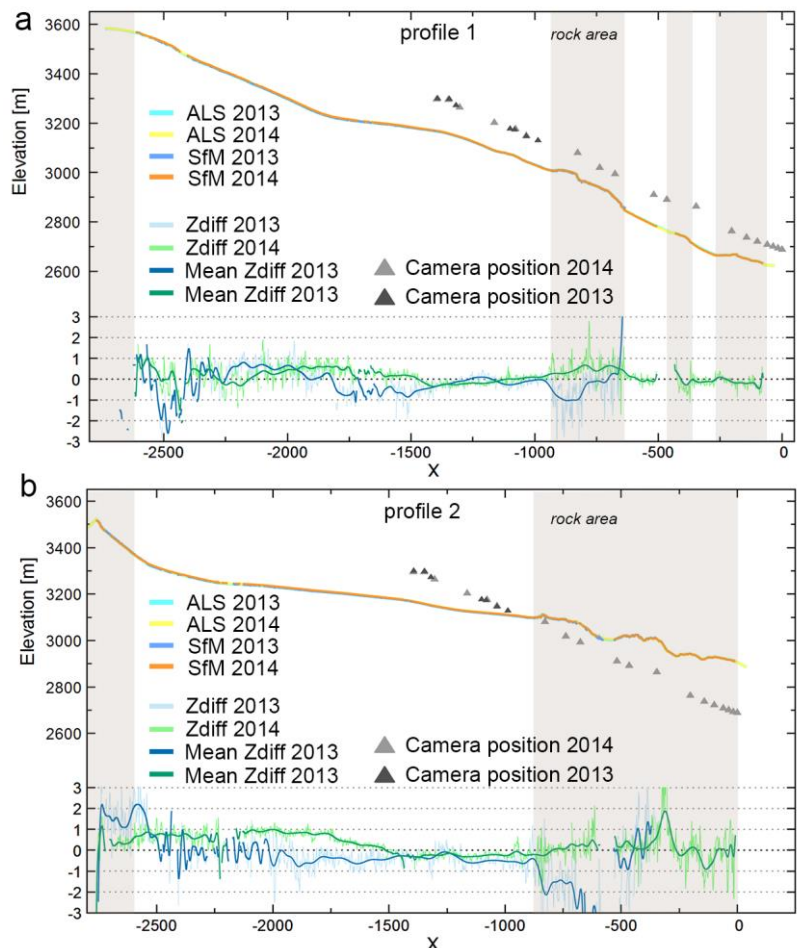
783
784 **Figure 4.** Workflow illustrating the photo-based 3D reconstruction process used in
785 this work for both case studies, starting from images collection to DEM generation.
786



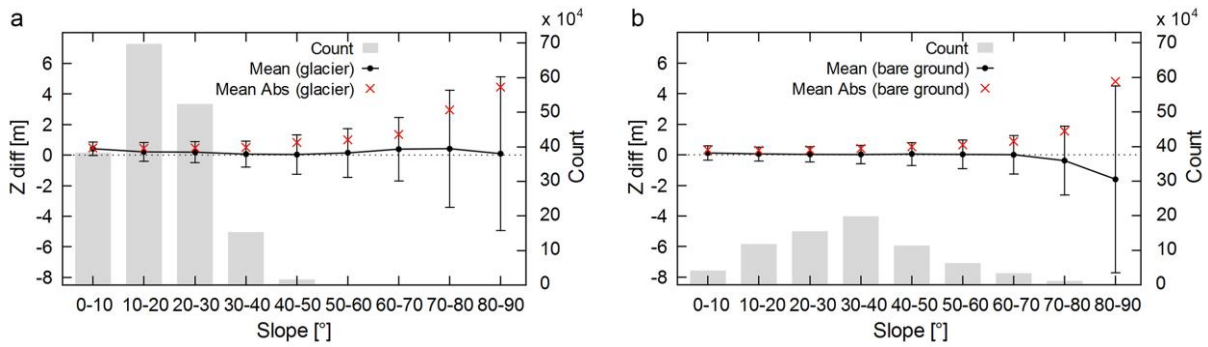
787
788 **Figure 5.** Hillshaded DEMs of La Mare glacier derived from photogrammetric
789 measurements on (a) 4 September 2013 and (b) 27 September 2014.
790



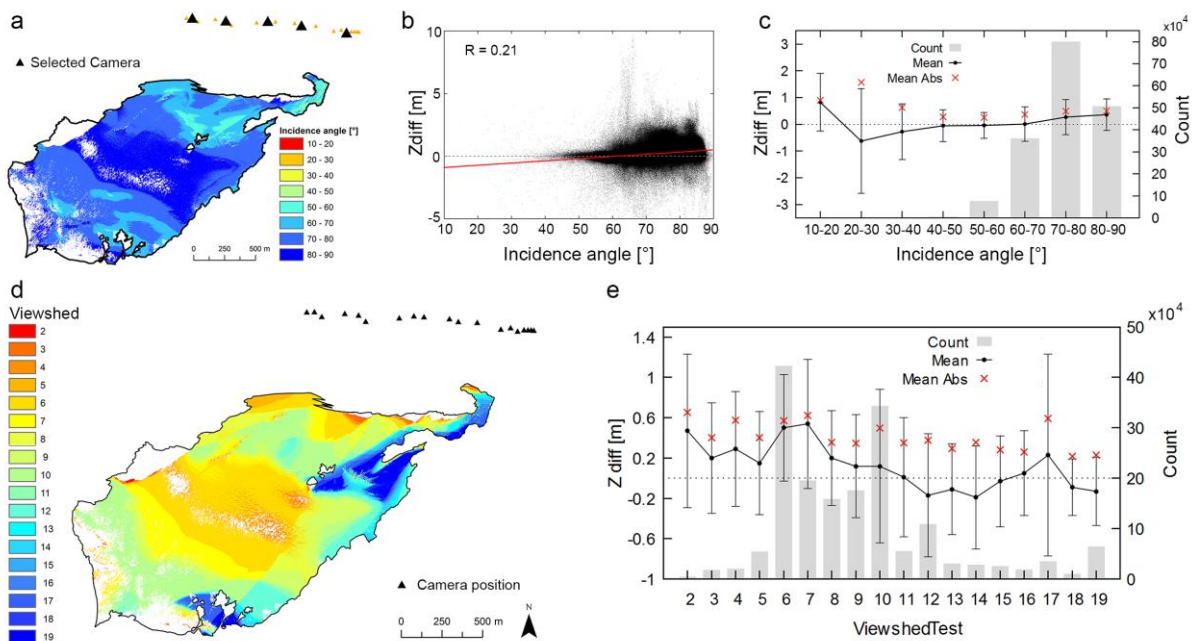
791
 792 **Figure 6.** Spatial distribution of elevation differences between photogrammetric and
 793 ALS-based DEMs on **(a)** 2013 and **(b)** 2014.



794
 795 **Figure 7.** Cross sections through the La Mare glacier DEMs show the glacier
 796 elevation change and the difference between 2013 and 2014 in SfM-MVS and ALS-
 797 based DEMs. The location of **(a)** the profile 1 and **(b)** profile 2 is indicated in Fig. 6.
 798 The x-axis zero has been fixed at the first camera position of the 2014 survey and the
 799 minimum and maximum values of the z-difference set to ± 3 m and both profiles and
 800 the camera positions were projected onto the xz-plan.



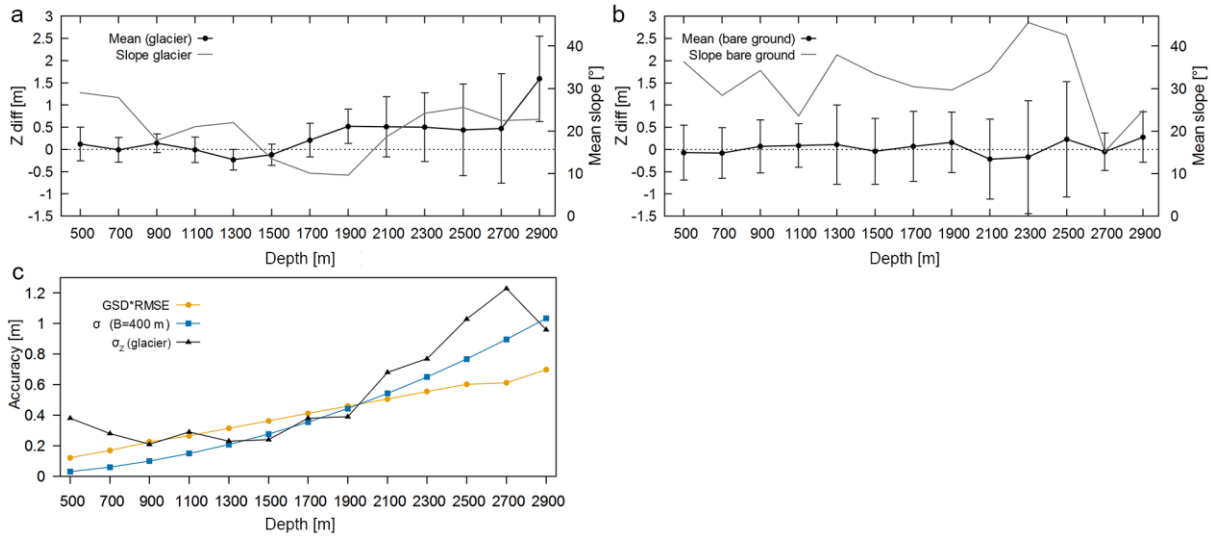
801
 802 **Figure 8.** Mean, mean of the absolute values and standard deviation of the 2014
 803 DoD between SfM-MVS and ALS-based DEM depending on slope calculated **(a)** in
 804 the glacier area and **(b)** in the bare ground outside glacier covered by rock. The grey
 805 bars show the count of cells at any given slope (y-axis on the right).



806
 807 **Figure 9.** Mean incidence angles between five cameras positions and vectors normal
 808 to the surface and viewshed analysis. **(a)** Map of the mean incidence angle
 809 calculated for five representative camera positions; **(b)** the scatterplot of the elevation
 810 difference and the mean incidence angle for the five camera positions; **(c)** mean with
 811 one standard deviation y bars and mean of the absolute value of elevation
 812 differences for the mean incidence angle intervals calculated for 5 selected camera;
 813 **(d)** map of the viewshed reconstructed area visible from all camera; **(e)** mean with
 814 one standard deviation y bars and mean of the absolute value of elevation
 815 differences for the viewshed reconstructed area.

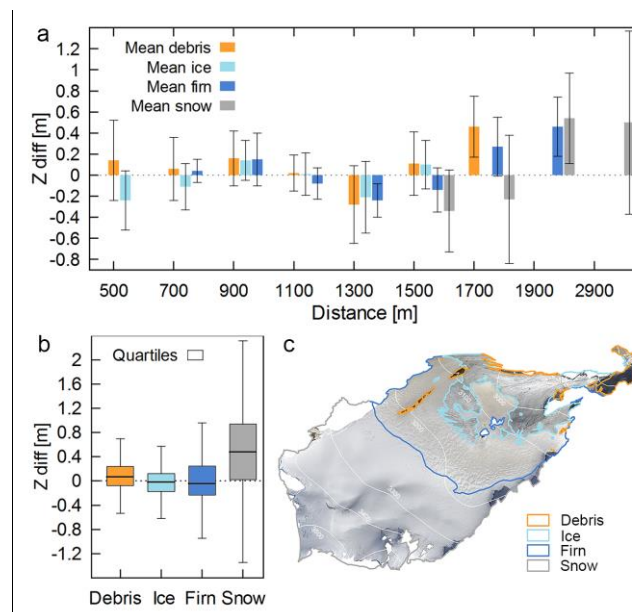
816

817



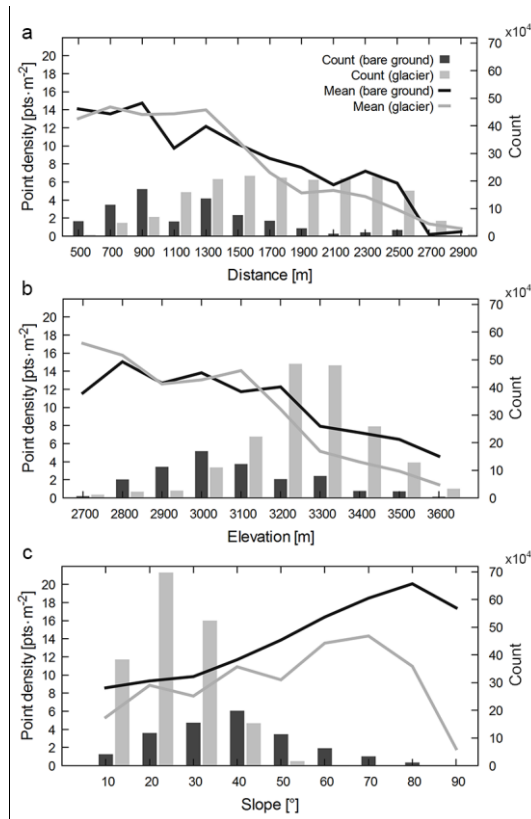
818

819 **Figure 10.** Mean and standard deviation of the 2014 DoD between SfM-MVS and
 820 ALS-based DEM depending on depth calculated **(a)** in the glacier area and **(b)** in the
 821 bare ground outside glacier covered by rock. The trend of the average slope angle
 822 for depth intervals is shown on the right y-axis. **(c)** Comparison of σ_z measured in the
 823 glacier reconstructed area, the theoretical depth accuracy estimated according to the
 824 Eq. (1) and the GSD multiplied for the GCPs RMSE for the depth intervals.

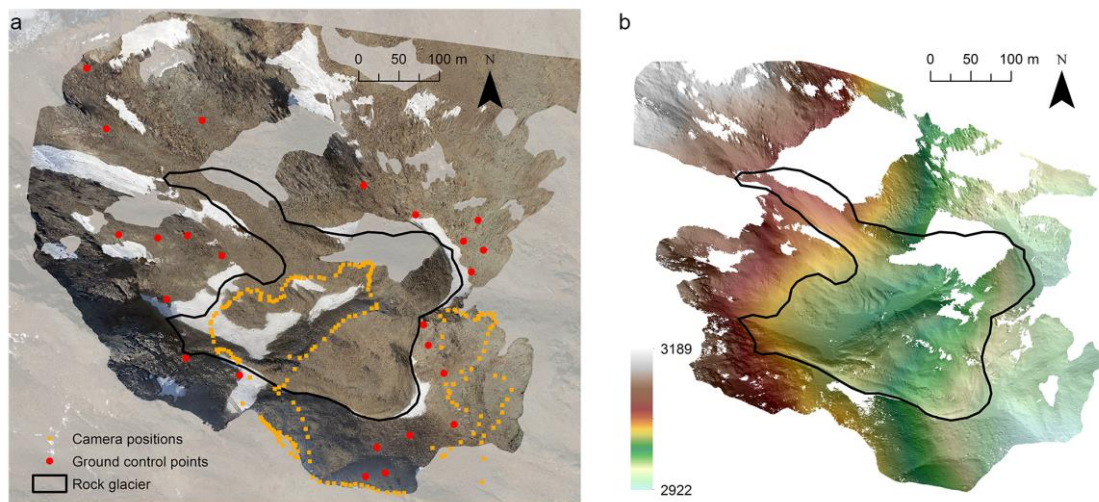


825

826 **Figure 11.** Elevation difference between the 2014 SfM-MVS and ALS-based DEMs
 827 calculated for different substrata. The figure shows **(a)** the mean and standard
 828 deviation of z-difference for four substrata (debris, ice, firn, and snow) grouped by
 829 distance from camera position; **(b)** the box plot of the z-difference for four substrata.
 830 In the box-whisker plot, values which exceeded $1.5 * IQR$ were considered outliers. In
 831 panel **(c)** the orthophoto of the glacier on 27 September 2014 and map of substrata.

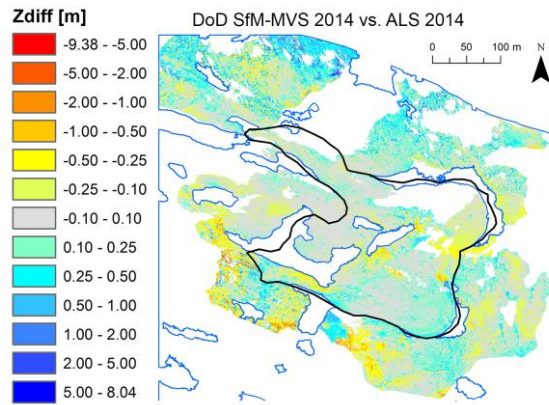


832 **Figure 12.** Relationships between point density of the 2014 photogrammetric 3D
 833 model and **(a)** camera-object distance, **(b)** elevation and **(c)** slope calculated for the
 834 glacier and rock stable area outside glacier. The point density was estimated using
 835 the filtered and subsampled point cloud.
 836



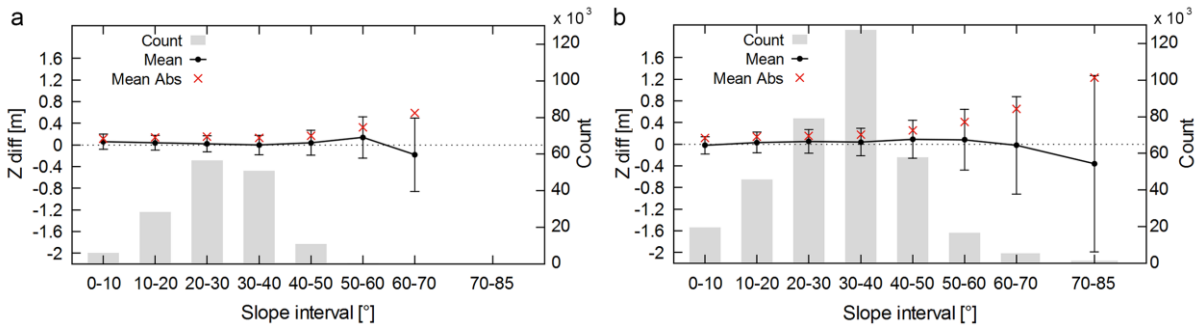
837 **Figure 13.** Correspondence between **(a)** the orthophoto of SfM-MVS 3D model of
 838 rock glacier surveyed on 27 September 2014 and **(b)** the hillshade model of rock
 839 glacier model calculated at the same data and hour of the images acquisition. The
 840 holes in the DEM represent not reconstructed area.
 841

842



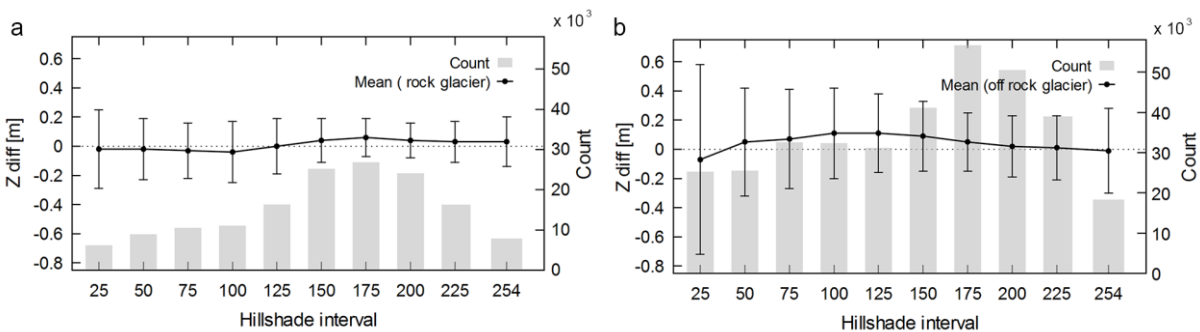
843
 844 **Figure 14.** Spatial distribution of elevation differences between photogrammetric and
 845 ALS-based DEM acquired on 27 September 2014 and 24 September 2014,
 846 respectively. The blue shape is the snow accumulation areas excluded during the
 847 DEMs comparison.

848

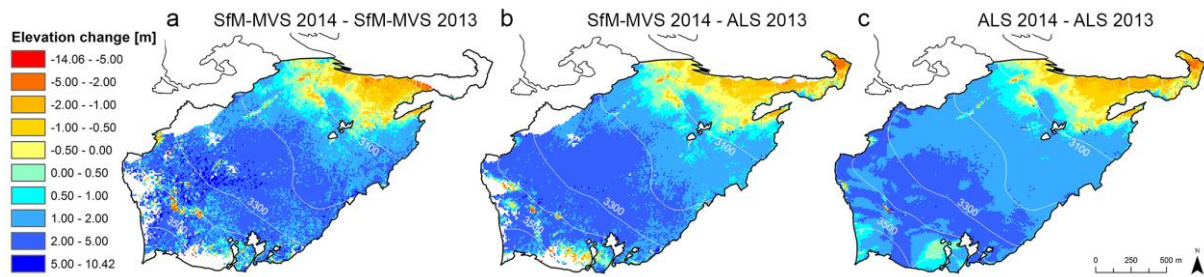


849
 850 **Figure 15.** Mean, mean of the absolute values and standard deviation of elevation
 851 differences between 2014 SfM-MVS and ALS-based DEMs calculated for the slope
 852 interval **(a)** in the rock glacier reconstructed area and **(b)** in the bare ground outside
 853 the rock glacier.

854

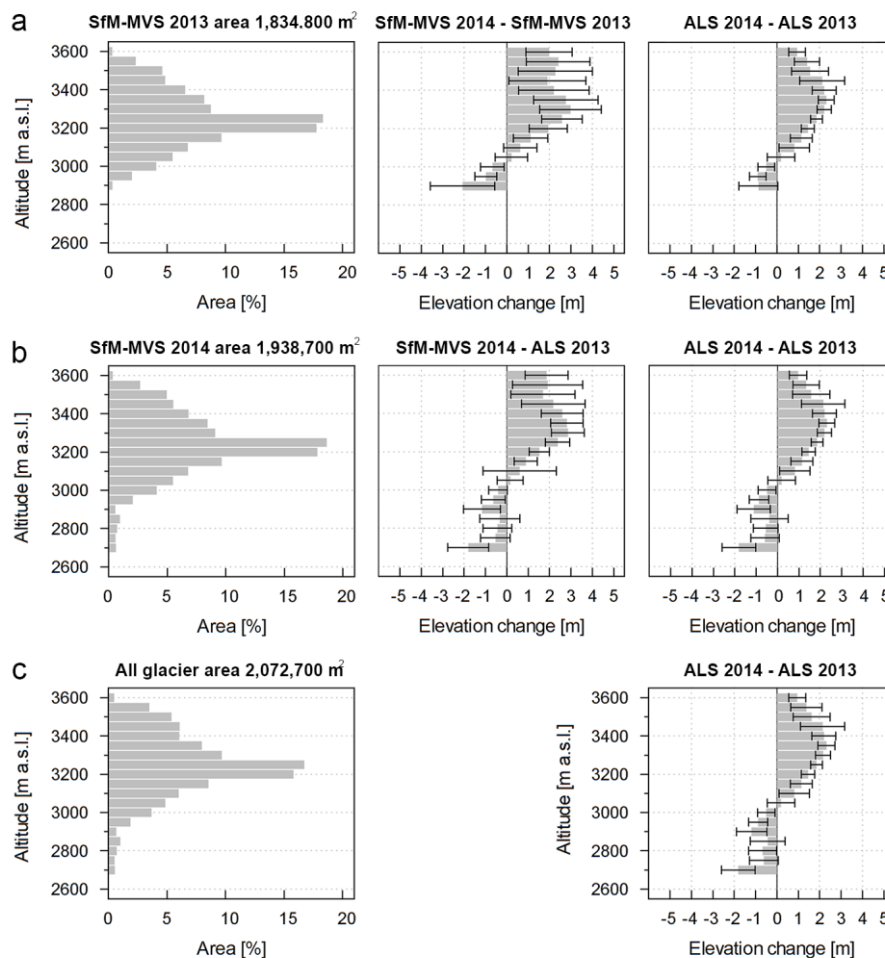


855
 856 **Figure 16.** Elevation differences between 2014 SfM-MVS and ALS-based DEMs
 857 calculated for the hillshade interval **(a)** in the rock glacier reconstructed area and **(b)**
 858 in the bare ground outside the rock glacier. Lowest values represent shadowed area
 859 whilst lighted areas present the highest values.



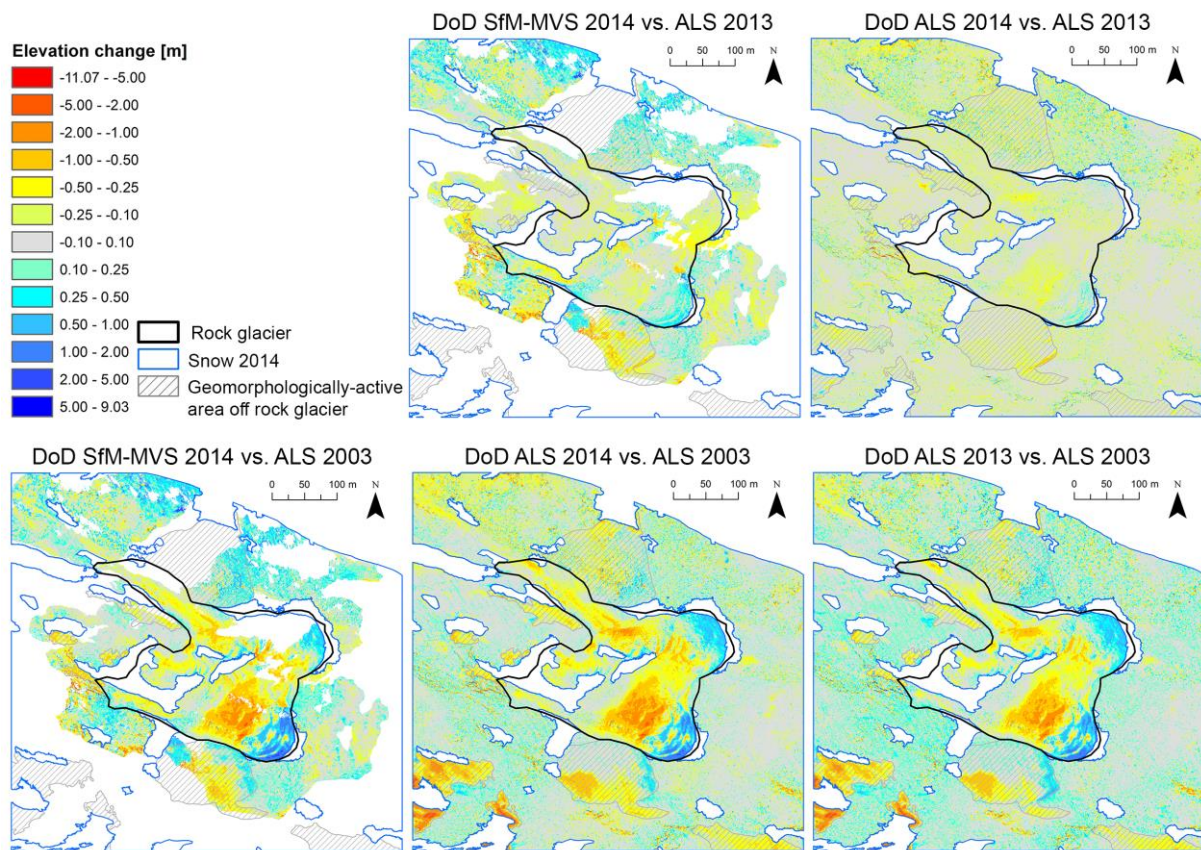
860

861 **Figure 17.** Spatial distribution of elevation changes between **(a)** Sfm-MVS 2014 and
 862 Sfm-MVS 2013 DEMs **(b)** Sfm-MVS 2014 and ALS 2013 over the area of the glacier
 863 with common coverage and **(c)** ALS 2014 and ALS 2013 over the entire glacier.

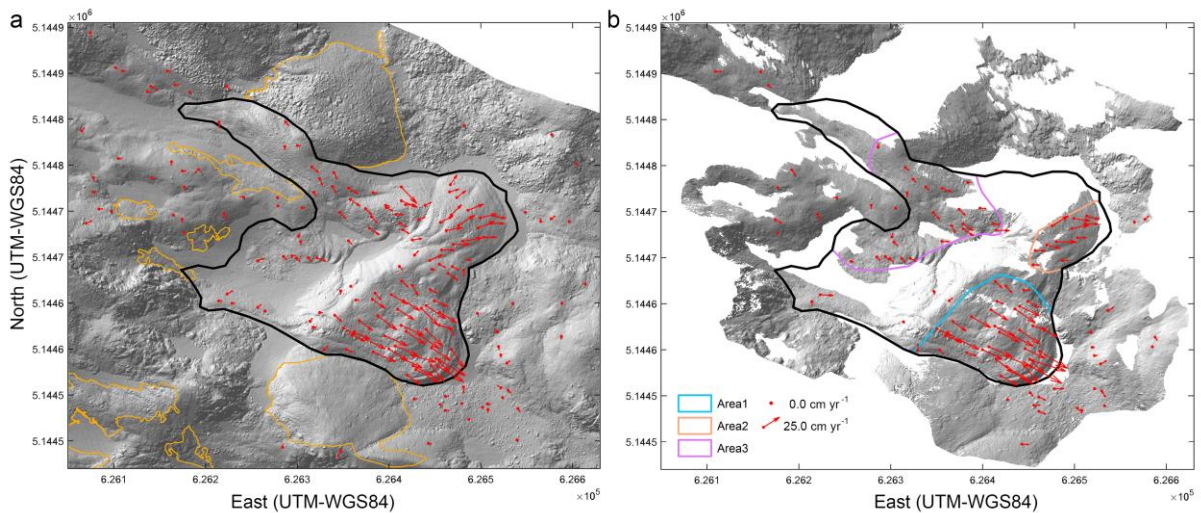


864

865 **Figure 18.** Area-altitude distribution and surface elevation change with standard
 866 deviation for the glaciological year 2014/2013 displayed for altitudinal bands with 50
 867 m interval. The elevation change were calculated between **(a)** Sfm-MVS DEMs of
 868 2013 and 2014 in the 2013 photogrammetric reconstructed area; **(b)** Sfm-MVS DEMs
 869 of 2014 and ALS DEM of 2014 in the 2014 photogrammetric reconstructed area; **(c)**
 870 ALS DEMs of 2013 and 2014 of the entire glacier. The photogrammetric results were
 871 compared with the corresponding ALS result calculated in the same area.



872
 873 **Figure 19.** Spatial distribution of elevation changes from September 2014 to
 874 September 2013 and September 2003 between the DEMs derived from SfM-MVS
 875 and ALS.



876
 877 **Figure 20.** Displacement vectors of the rock glacier between 2003 and 2014
 878 computed by a manual identification of natural features visible in the shaded DEMs
 879 generated by (a) ALS for both survey epochs and by (b) ALS and photogrammetry
 880 for 2003 and 2014 survey, respectively.